LIDAR-DRIVEN SPATIAL REGULARIZATION FOR HYPERSPECTRAL UNMIXING

Tatsumi Uezato[(1)]*, Mathieu Fauvel*[(2)] *and Nicolas Dobigeon*[(1)]

[(1)] University of Toulouse, IRIT/INP-ENSEEIHT, 31071 Toulouse, France
[(2)] University of Toulouse, Dynafor/INP-ENSAT, 31326 Castanet-Tolosan, France
firstname.lastname@enseeiht.fr, mathieu.fauvel@ensat.fr

ABSTRACT

Only a few research works consider LiDAR data while conducting hyperspectral image unmixing. However, the digital surface model derived from LiDAR can provide meaningful information, in particular when spatially regularizing the inverse problem underlain by spectral unmixing. This paper proposes a general framework for spectral unmixing that incorporates LiDAR data to inform the spatial regularization applied to the abundance maps. The proposed framework is validated and compared to existing unmixing methods that incorporate spatial information derived from the hyperspectral image itself using two different simulated data and digital surface models. Results show that the spatial regularization incorporating LiDAR data significantly improves abundance estimates.

***Index Terms*—** Hyperspectral imagery, spectral unmixing, edge, lidar, classification

1. INTRODUCTION

Due to a relatively low spatial resolution of the sensors, hyperspectral images are generally composed of *mixed pixels*, i.e., composed by spectral mixtures of several elementary materials in unknown proportions. Spectral unmixing aims at deconvolving the spectral mixtures into a collection of reference spectra, known as *endmembers*, and their corresponding proportions or *abundances* [1]. Most of conventional spectral unmixing methods ignore the intrinsic 2D+λ structure of the hyperspectral datacube (where λ refers to the wavelength) but exploit only the spectral information. However, recent advances in spectral unmixing enable spatial information to be incorporated into the unmixing process [2, 3]. The key idea consists in promoting identical or similar abundance estimates in a given neighborhood of the pixels of interest. This strategy relies on the assumption that neighboring pixels generally show smooth transitions in abundances. These methods incorporate this spatial information as a regularization to describe the spatial variations of abundances in a local neighborhood [4, 5].

One of the well-known limitations of spatial regularizations consists in not properly preserving the edges between homogeneous areas, even when using total variation (TV)-like penalizations. Instead, they tempt to overly smooth edges, finally leading to poor abundance estimates in these specific areas. One solution is to build a so-called *guidance map* which localizes these edges. The spatial regularization for these pixels can be subsequently adjusted accordingly, by resorting to a *weighted* spatial regularization [6]. This side information is commonly estimated from the hyperspectral image to be unmixed directly. However, this estimation may be greatly affected by noise or illumination variations [7], which may lead to incorrect weighting of the spatial regularization. One alternative consists in exploiting external data, if available, to derive this guidance map. Such strategy is expected to be robust to the aforementioned problem. In particular, LiDAR data have a great potential to extract complementary spatial information that can be used to derive a reliable guidance map. Indeed, LiDAR data can discriminate different materials and/or areas using height information, even if they are spectrally similar [8]. Due to its intrinsic nature, it is robust to any illumination variations during the acquisition. While LiDAR data have been successfully used for hyperspectral image classification, only a few studies proposed to exploit LiDAR data for spectral unmixing. In [9], the authors investigated whether weighting the spatial regularization thanks to the LiDAR data can improve the accuracy when estimating abundances, especially in shaded pixels. However, it is still unclear whether LiDAR data or a combination of LiDAR data and another guidance map can lead to more accurate estimates of abundances. This paper proposes to fill this gap.

More precisely, the contributions of this paper are twofold: 1) to develop a new spectral unmixing framework that incorporates LiDAR data into the weighting of the spatial regularization; and 2) to conduct a comprehensive comparison of the weighting functions derived from LiDAR data or from its combination with another guidance map. The proposed framework has been validated using two simulated data to as-

Part of this work has been funded by EU FP7 through the ERANETMED JC-WATER program, MapInvPlnt Project ANR-15-NMED-0002-02 and by the MUESLI IDEX ATS project, Toulouse INP.

sess whether LiDAR data can lead to significant improvement of abundance estimates.

2. LIDAR DATA-DRIVEN UNMIXING

2.1. Unmixing with spatial regularizations

The linear mixture model (LMM) has been widely used to decompose a mixed spectrum into a collection of endmembers and their abundances. LMM represents a mixed spectrum as a linear combination of the endmember spectra

$$\mathbf{y}_i = \mathbf{S}\mathbf{a}_i + \mathbf{n}_i \tag{1}$$

where $\mathbf{y}_i \in \mathbb{R}^{L\times 1}$ is a mixed spectrum of the ith pixel, $\mathbf{S} \in \mathbb{R}^{L\times M}$ is the matrix of endmember signatures, $\mathbf{a}_i = [a_{1i}, \ldots, a_{Mi}]^T \in \mathbb{R}^{M\times 1}$ represents abundance fractions at the ith pixel, $\mathbf{n}_i \in \mathbb{R}^{L\times 1}$ represents noise or modeling error, L is the number of spectral bands and M is the number of endmembers. Abundance non-negativity constraint (ANC) and the abundance sum-to-one constraint (ASC) are usually imposed as follows

$$\forall m, i,\ a_{mi} \geq 0 \quad \text{and} \quad \forall i,\ \sum_{m=1}^{M} a_{mi} = 1. \tag{2}$$

When endmembers $\mathbf{S}$ have been identified thanks to *a priori* knowledge or extracted from the hyperspectral image using a dedicated endmember extraction algorithm [1], the abundance vectors $\mathbf{a}_i$ ($i = 1, \ldots, N$) can be estimated pixel-by-pixel by solving the N following optimization problems, where N is the number of pixels,

$$\min_{\mathbf{a}_i} \frac{1}{2}\|\mathbf{y}_i - \mathbf{S}\mathbf{a}_i\|_2^2 \quad \text{s.t.} \quad (2). \tag{3}$$

In the optimization problem, abundances are estimated for each pixel independently, ignoring the spatial information inherent to the abundance maps to be recovered. One conventional way to regularize the associated inverse problem consists in incorporating a spatial regularization into the minimization problem, leading to

$$\min_{\mathbf{a}_i} \frac{1}{2}\|\mathbf{y}_i - \mathbf{S}\mathbf{a}_i\|_2^2 + \lambda \sum_{j\in\mathcal{N}(i)} w_{ij}\|\mathbf{a}_i - \mathbf{a}_j\|_p^p \text{ s.t. } (2) \tag{4}$$

where λ is a parameter to control the balance between the data fitting term and the spatial regularization, $\mathcal{N}(i)$ is the set of the neighboring pixels[1] of the ith pixel, w_{ij} is a weight describing the expected similarity between the ith and jth pixels. Popular ℓ_p-norms considered in spatial regularizations include $p = 2$ and $p = 1$, which promotes smooth variations and piecewise constant behaviors of the abundance maps, respectively. In this work, without loss of generality of the main contribution presented in this paper, the case $p = 1$ will be considered. Moreover, when the weights are tuned to $w_{ij} = 1$ ($\forall i, j$) with $p = 1$, the resulting spatial regularization is known as a specific instance of the total variation (TV) penalization. In this case, each neighboring pixel equally contributes to the spatial regularization term. However, this may be inappropriate, in particular for pixels located in edges between several distinct areas characterized by different materials and/or composition. Thus, choosing appropriate weights describing the spatial relationships between neighboring pixels can greatly improve abundance estimates [6]. The w_{ij} can be adjusted according to a guidance image which summarizes this spatial information, such as the edge locations. This guidance image can be derived directly from the hyperspectral image to be unmixed. However, this choice can be significantly affected by variations in illumination or sensor noise. Moreover, when distinct areas are composed of spectrally similar materials, such a guidance map will hardly be able to encode the presence of edges. Conversely, digital surface model (DSM) computed from LiDAR data represents a great opportunity to overcome these limitations. If the height derived from DSM is different for each region belonging to a particular mixture of endmembers, DSM can correctly extract the edge information even under different illumination conditions. This property is particularly useful in urban or vegetated areas where the height of materials plays an important role [8, 10]. In what follows, various guidance maps are presented, based on the hyperspectral image, DSM or a combination of both. Then, the spatially regularized optimization problem is solved using the alternating direction method of multipliers, following the strategy in [4]. More information regarding the optimization procedure is given in [11].

[1] In this study, a 4-order neighborhood will be considered.

2.2. Different types of weights

A variety of guidance images can be used to adjust the weights in the spatial regularization. In this section, five different approaches are described. Each weight is calculated by using a normalized squared difference of features between a target pixel and the neighborhood pixels.

w-HI: Weights are chosen from the spectral similarity between neighboring pixels

$$w_{ij} = \frac{1}{Q_i} \exp\left(-\frac{1}{\sigma_y^2}\frac{\|\mathbf{y}_i - \mathbf{y}_j\|_2^2}{\|\mathbf{y}_i + \mathbf{y}_j\|_2^2}\right) \tag{5}$$

where $\mathbf{y}_i$ is the spectrum of the ith pixel and σ_y^2 is a parameter controlling the weight range and Q_i represents the normalization constant such that $\sum_{j\in\mathcal{N}(i)} w_{ij} = 1$.

w-PC1: Weights are adjusted from the similarity between pixels of the first principal component (PC) recovered by PC analysis

$$w_{ij} = \frac{1}{Q_i} \exp\left(-\frac{1}{\sigma_p^2}\frac{(p_i - p_j)^2}{(p_i + p_j)^2}\right). \tag{6}$$

where p_i is the value of the ith pixel of the first PC1 and σ_p^2 is a parameter controlling the weight range.

w-DSM: When DSM derived from LiDAR data is available, the guidance map can be computed from the similarity between the heights of neighboring pixels

$$w_{ij} = \frac{1}{Q_i} \exp\left(-\frac{1}{\sigma_h^2} \frac{(h_i - h_j)^2}{(h_i + h_j)^2}\right). \quad (7)$$

where h_i is the height of the ith pixel and σ_h^2 is a parameter controlling the weight range. Moreover, this DSM information can be combined with the previous guidance maps, as detailed in what follows.

w-HI-DSM: Coupling DSM with previous guidance maps computed from the hyperspectral image leads to

$$w_{ij} = \frac{1}{Q_i} \left[\exp\left(-\frac{1}{\sigma_y^2} \frac{\|\mathbf{y}_i - \mathbf{y}_j\|_2^2}{\|\mathbf{y}_i + \mathbf{y}_j\|_2^2}\right) + \exp\left(-\frac{1}{\sigma_h^2} \frac{(h_i - h_j)^2}{(h_i + h_j)^2}\right)\right].$$

w-PC1-DSM: Similarly, the weights can be adjusted as

$$w_{ij} = \frac{1}{Q_i} \left[\exp\left(-\frac{1}{\sigma_p^2} \frac{(p_i - p_j)^2}{(p_i + p_j)^2}\right) + \exp\left(-\frac{1}{\sigma_h^2} \frac{(h_i - h_j)^2}{(h_i + h_j)^2}\right)\right].$$

3. EXPERIMENTS

3.1. Experiment using simulated data 1 (SIM1)

Generation of SIM1: SIM1 has been generated to assess whether the weighting function derived from DSM can improve the abundance estimates in the specific situations when each spatially coherent region is characterized by a different height. The simulated hyperspectral image and DSM data have been generated as follows. Five endmember spectra have been randomly selected from the USGS spectral library. A synthetic 100×100 discrete-value image has been randomly generated as in [12] to identify spatially coherent areas. Each area is assigned a different height to build synthetic DSM (Fig. 1a). Within each area, statistically consistent synthetic mixtures of the $M = 5$ endmembers are randomly generated, and then corrupted by an additive Gaussian noise leading to a signal-to-noise ratio $\mathrm{SNR} = 20$dB. A color composition of the resulting hyperspectral image is depicted in Fig. 1b.

Validation of methods: Quantitative validation has been conducted using the root mean square error (RMSE) of the abundance estimates

$$\mathrm{RMSE} = \sqrt{\frac{1}{NM} \sum_{i=1}^{N} \sum_{m=1}^{M} (a_{mi} - \hat{a}_{mi})^2} \quad (8)$$

where a_{mi} and $\hat{a}_{mi}$ are the actual and estimated abundance fractions. This quantitative analysis can be also conducted by restricting the computation of RMSE for the pixels specifically localized in the edge areas of the hyperspectral image. Interested readers are invited to consult [11] for details.

Results: For the weighting functions proposed in Section 2.2, RMSE as functions of the regularization parameter λ are depicted in Fig. 2. As expected, RMSE estimated from

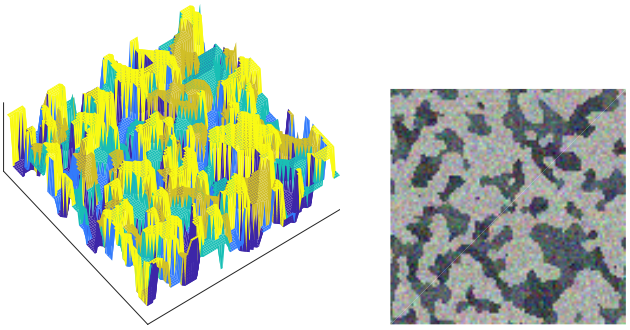

(a) (b)

Fig. 1: SIM1: (a) Synthetic DSM. (b) Color composition of the synthetic hyperspectral data.

no-weight performs poorly compared to other methods incorporating DSM information. In particular, RMSE of the no-weight approach significantly decrease for large values of λ. This shows that this method is very sensitive to the value of the regularization parameter λ. Conversely, the methods that incorporate DSM information perform favorably. The methods estimate accurate abundances even when a large value (>1) of λ is chosen. Among all these methods, those relying on DSM perform better than their DSM-free counterparts. This shows that the use of DSM can lead to more accurate estimates of abundances especially where the height allows spatially discrete regions to be distinguished.

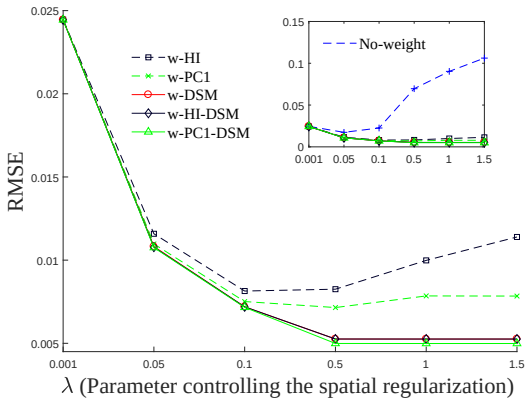

Fig. 2: SIM1: Abundance RMSE as a function of λ.

3.2. Experiment using simulated data 2 (SIM2)

Generation of SIM2: This second experiment has been designed to assess whether DSM can still be useful for estimating abundances when DSM describes only partially the spatial information. To do so, a synthetic yet more realistic hyperspectral image has been generated and coupled with real DSM. More precisely, a real hyperspectral image and its cor-

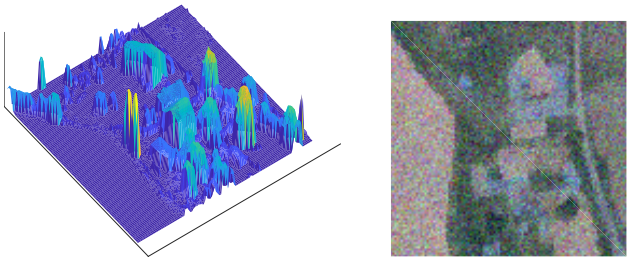

(a) (b)

Fig. 3: SIM2: (a) Real DSM. (b) Color composition of the synthetic hyperspectral data.

responding DSM (depicted in Fig. 3a) have been acquired during a flight campaign conducted in June 2016, over the city of Saint-André, France. First, $M = 4$ endmembers have been extracted from this real image using the n-Dimensional Visualizer provided by the ENVI software. To build ground-truth abundance maps, this real hyperspectral image has been unmixed following the LMM. Finally, based on these endmember spectra and abundance maps, the synthetic hyperspectral image referred to as SIM2 is generated according to LMM and corrupted by an additive Gaussian noise with SNR= 20dB (see Fig. 3b).

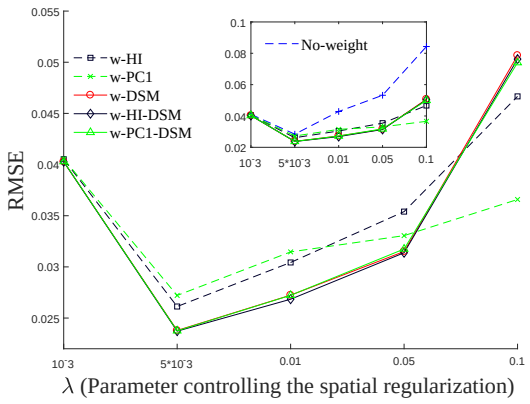

Fig. 4: SIM2: Abundance RMSE as a function of λ.

Results: RMSE is depicted as a function of the regularization parameter in Fig. 4. The method with no weight performs poorly compared with other methods that incorporate edge information. RMSE obtained by the w-DSM unmixing model is smaller than those derived from w-PC1 or w-HI when an optimal value of λ is used. The combinations of DSM and other guidance images (w-PC1-DSM and w-HI-DSM) also show smaller RMSE than those derived from the DSM-free methods (w-HI or the w-PC1) for a wide range of λ. However, RMSE derived from the DSM-informed methods are larger for a large value of the regularization parameter, i.e., when the unmixing problem is more spatially regularized. This is probably due to the fact that DSM does not capture all the spatial information.

4. CONCLUSION

In this study, a new spectral unmixing framework that incorporates DSM information derived from LiDAR data was proposed. The proposed method was compared to the methods incorporating spatial information derived from the hyperspectral image directly. Results showed that the use of LiDAR data with other guidance maps can lead to significant improvement of abundance estimation and robustness.

5. REFERENCES

[1] J. M. Bioucas-Dias, A. Plaza, N. Dobigeon, M. Parente, D. Qian, P. Gader, and J. Chanussot, "Hyperspectral unmixing overview: Geometrical, statistical, and sparse regression-based approaches," *IEEE J. Sel. Topics Appl. Earth Observations Remote Sens.*, vol. 5, no. 2, pp. 354–379, 2012.

[2] O. Eches, N. Dobigeon, and J. Y. Tourneret, "Enhancing hyperspectral image unmixing with spatial correlations," *IEEE Trans. Geosci. Remote Sens.*, vol. 49, no. 11, pp. 4239–4247, 2011.

[3] C. Shi and L. Wang, "Incorporating spatial information in spectral unmixing: A review," *Remote Sens. Environment*, vol. 149, no. 0, pp. 70–87, 2014.

[4] M. D. Iordache, J. M. Bioucas-Dias, and A. Plaza, "Total variation spatial regularization for sparse hyperspectral unmixing," *IEEE Trans. Geosci. Remote Sens.*, vol. 50, no. 11, pp. 4484–4502, 2012.

[5] T. Uezato, R. J. Murphy, A. Melkumyan, and A. Chlingaryan, "Incorporating spatial information and endmember variability into unmixing analyses to improve abundance estimates," *IEEE Trans. Image Process.*, vol. 25, 2016.

[6] J. Liu, J. Zhang, Y. Gao, C. Zhang, and Z. Li, "Enhancing spectral unmixing by local neighborhood weights," *IEEE J. Sel. Topics Appl. Earth Observations Remote Sens.*, vol. 5, no. 5, pp. 1545–1552, 2012.

[7] T. Uezato, R. J. Murphy, A. Melkumyan, and A. Chlingaryan, "A novel spectral unmixing method incorporating spectral variability within endmember classes," *IEEE Trans. Geosci. Remote Sens.*, vol. 54, no. 5, pp. 2812–2831, 2016.

[8] L. Ni, L. Gao, S. Li, J. Li, and B. Zhang, "Edge-constrained markov random field classification by integrating hyperspectral image with lidar data over urban areas," *Journal of Applied Remote Sensing*, vol. 8, no. 1, pp. 085 089–085 089, 2014.

[9] A. Castrodad, T. Khuon, R. Rand, and G. Sapiro, "Sparse modeling for hyperspectral imagery with lidar data fusion for subpixel mapping," in *Proc. IEEE Int. Conf. Geosci. Remote Sens. (IGARSS)*, 2012, pp. 7275–7278.

[10] M. Dalponte, L. Bruzzone, and D. Gianelle, "Fusion of hyperspectral and lidar remote sensing data for classification of complex forest areas," *IEEE Trans. Geosci. Remote Sens.*, vol. 46, no. 5, pp. 1416–1427, 2008.

[11] T. Uezato, M. Fauvel, S. May, and N. Dobigeon, "Hyperspectral image unmixing with LiDAR data-aided spatial regularization," submitted. [Online]. Available: http://arxiv.org/abs/1712.07862/

[12] T. Uezato, R. J. Murphy, A. Melkumyan, and A. Chlingaryan, "A novel endmember bundle extraction and clustering approach for capturing spectral variability within endmember classes," *IEEE Trans. Geosci. Remote Sens.*, vol. 54, no. 11, 2016.